Mon. Not. R. Astron. Soc. **359,** 383–400 (2005) doi:10.1111/j.1365-2966.2005.08903.x

The dark lane of the planetary nebula NGC 6302★†

M. Matsuura,[1]‡ A. A. Zijlstra,[1] F. J. Molster,[2] L. B. F. M. Waters,[3,4] H. Nomura,[1,5] R. Sahai[6] and M. G. Hoare[7]

[1]*Department of Physics and Astronomy, University of Manchester, Sackville Street, PO Box 88, Manchester M60 1QD*
[2]*ESTEC, European Space Agency, Keplerlaan 1, 2201 AZ Noordwijk, The Netherlands*
[3]*Astronomical Institute 'Anton Pannekoek', University of Amsterdam, Kruislaan 403, 1098 SJ, Amsterdam, The Netherlands*
[4]*Instituut voor Sterrenkunde, Katholieke Universiteit Leuven, Celestijnenlaan 200B, 3001 Heverlee, Belgium*
[5]*Department of Earth and Planetary Science, Graduate School of Science and Technology, Kobe University, Kobe 657-8501, Japan*
[6]*Jet Propulsion Laboratory, California Institute of Technology, MS 183-900, 4800 Oak Grove Drive, Pasadena, CA 91109, USA*
[7]*Department of Physics and Astronomy, University of Leeds, Leeds LS2 9JT*

Accepted 2005 February 4. Received 2005 February 3; in original form 2004 November 24

ABSTRACT

The butterfly-shaped planetary nebula, NGC 6302, shows a unique, dense equatorial dark lane, which is presumably a dusty disc, obscuring an unobserved, very hot central star. We trace the structure of this disc using *Hubble Space Telescope* Hα and [N II] images, Very Large Telescope L-and M-band images at 0.4-arcsec resolution, including Brα and polycyclic aromatic hydrocarbon (PAH) images, and a James Clerk Maxwell Telescope 450-μm image. Extinction maps are derived from these images. Within the disc, the extinction is $A_{\rm H\alpha}$ = 5–7 mag and $A_{\rm Br\alpha}$ = 1–2 mag. The 450-μm map shows a north–south elongated central core, tracing the massive dust disc, and extended emission from dust in the bipolar flows. A fit to the spectral energy distribution yields the disc dust mass of 0.03 $M_\odot$. The innermost region shows an ionized shell. The orientation of the polar axis shows a marked change between shell, disc and inner and outer outflow. The structures are well described by the warped-disc model of Icke (2003). PAH images are presented: PAH emission is found in the shell but avoids the disc. An infrared source is found close to the expected location of the central star.

Key words: dust, extinction – ISM: jets and outflows – planetary nebulae: individual: NGC 6302.

1 INTRODUCTION

A planetary nebula (PN) originates when a low- or intermediate-mass star (1–8 $M_\odot$) expels 20–80 per cent of its mass, and the resulting circumstellar shell becomes ionized. The ejection occurs during the asymptotic giant branch (AGB), when during a brief phase of 10^3–10^4 yr, mass-loss rates are as high as 10^{-7}–10^{-4} $M_\odot$ yr^{-1}. PNe commonly show axis-symmetric shapes, such as elliptical, bipolar or multipolar (e.g. Sahai & Trauger 1998; Balick & Frank 2002). The shapes indicate deviations from spherical symmetry in the original wind. During the post-AGB phase, when the star rapidly increases in temperature and surface gravity, a developing fast wind from the central star compresses the ejecta (Kwok 1982), and in the process amplifies any asymmetry already present (Icke 1988). But there is so far limited evidence of axis-symmetric outflows in AGB stars (e.g. Zijlstra 2001a; Zijlstra et al. 2001b; Sahai et al. 2003), leaving the origin open. A catastrophic change from spherically symmetric mass loss to axis-symmetric mass loss at the very end of the AGB is often postulated.

The most extreme bipolar morphologies appear to be related to circumstellar discs (Balick 1987). Icke (2003) has suggested that multipolar PNe originate when a fast wind compresses a warped, molecular disc. Around cooler post-AGB stars, discs appear to originate when a close binary captures part of the ejecta (e.g. Van Winckel et al. 1999). Such thin, keplerian discs are not uncommon around cool post-AGB stars but are rarely found around PNe. Many PNe show dense torii, but whether these evolve from post-AGB circumbinary discs is not yet known. They could also come from equatorially enhanced mass loss on the AGB, and present a different evolutionary sequence from that of the close binaries. A problem is that few PNe discs or torii have been well parameterized.

NGC 6302 is one of the few examples of an evolved, hot star still retaining a disc. The undetected central star is believed to be

★Based on observations made with the NASA/ESA *Hubble Space Telescope*, obtained from the ESA/ECF Data Archive. *HST* is operated by the Association of Universities for Research in Astronomy, Inc., under NASA Contract No. NASA 5-26555. These observations are associated with Program No. 8345.
†Based on observations with the European Southern Observatory, Very Large Telescope using ISAAC (proposal numbers 65.D-0395A and 73.D-0359A).
‡E-mail: m.matsuura@manchester.ac.uk

one of the hottest PN central stars known (Pottasch et al. 1996). NGC 6302 is known as the prototypical 'butterfly' PN, with the fast wind channelled into two 'wings' by a central dense structure. This structure is seen as a dark lane extending from north to south, perpendicular to the wings. But the inner ionized region, as seen in the 6-cm radio continuum, shows a toroidal structure which is inclined at about 45 degrees to the optical major axis (Gómez et al. 1989). The structure of the inner nebula, with its potentially multiple axes, is therefore still under discussion.

In this paper we present deep optical and infrared images of NGC 6302, with subarcsecond resolution, aimed at resolving the inner nebula and the obscuring disc. The dust from this disc is also detected in thermal far-infrared emission.

We adopt a distance of 1 kpc, following Kemper et al. (2002, 0.91 kpc). Previous distance estimates range from 0.15–2.4 kpc (Meaburn & Walsh 1980; Rodríguez & Moran 1982); Gómez et al. (1989) derives an expansion distance of 2.2 kpc, but this method can be questioned for highly asymmetric nebulae. Distances much larger than 1 kpc lead to very high values for luminosity and shell mass.

2 OBSERVATIONS

2.1 *HST* optical observations

Hubble Space Telescope (*HST*) images were obtained from the data archives at the Space Telescope–European Coordinating Facility (ST–ECF). The data were taken on 2000 February 21 with Wide Field Planetary Camera 2 (WFPC2), which has four 800×800 pixel detectors. The pixel scale is 0.046 arcsec for the Planetary Camera, which covers the central region of the nebula, and 0.1 arcsec for the three Wide Field Cameras. Two filters were used, with exposure times of 610 s (two 300-s frames and one 10-s frame) for the F656N filter and 470 s (two 230-s frames and one 10-s frame) for F658N. The F656N filter (central wavelength 6564 Å, width 21.5 Å) mainly traces Hα emission, although some 6548 and 6584 Å [N II] emission is included in the passband (cf. Dudziak & Walsh 1997). The F658N image (λ_0 = 6590 Å, $\Delta\lambda_0$ = 28.5 Å) suggests that 6584 Å [N II] emission may contribute up to 10 per cent of the inband flux of F656N image. Here, we use the F656N image as an Hα image and F658N as an [N II] image. Pipeline-reduced data were used. The intensities are calibrated using the PHOTFLAM header parameter. Cosmic rays were removed by comparing four individual frames for the same region. The reduced Hα image is shown in Fig. 1.

The *HST* images suffer from distortion. We use the parameters in Anderson & King (2003) to obtain the corrected coordinate of each pixel. Triangular linear interpolation is used to reconstruct the distortion-corrected image with a 0.071 arcsec grid, which is the same grid size as the infrared images discussed below. This correction is calculated only for the central region compared with other images.

2.2 Near-infrared images

Near-infrared images of NGC 6302 were taken with ISAAC (Moorwood et al. 1999) at the ESO Very Large Telescope (VLT). The data were acquired on 2000 August 15, in service mode. The weather was clear. Filters used are summarized in Table 1; the obtained images are shown in Figs 2 and 3. The 3.28-μm narrow (NB_3.28) covers the PAH band with some contamination from Pfδ and He I 6–7, and the 4.07-μm narrow band (NB_4.07) contains the Brα line. There is no strong emission line known in the wavelength ranges of the narrow M band (M_NB) and the 3.21-μm narrow band (NB_3.21) (e.g. Beintema & Pottasch 1999) and these bands represent continuum emission. The background was subtracted by chopping and nodding to a position 30 arcsec to the north-west, while keeping the source on the array. Chopping frequency is 0.47–0.45 Hz depending on the bands. Some negative images of nearby stars apparent inside NGC 6302 are owing to chopping (Fig. 3). Jittering was used to improve flat-fielding. The total exposure times were 841 s in M_NB, 217 s in NB_3.21, 287 s in NB_3.28, and 411 s in NB_4.07, respectively. The pixel scale is 0.071 arcsec.

The full width half maximum (FWHM) in the frames, measured from a nearby star, ranges between 0.3 and 0.4 arcsec. (The zenith optical seeing during the observations varied between 0.4 and 0.85 arcsec.) Some image elongation is seen in the M band, which could be owing to the filter (ISAAC manual). The results are summarized in Table 1.

We used ECLIPSE and IDL for the data reduction. Detector non-linearity, which is significant at the brighter range, was corrected according to the measurements of the ISAAC instrument team. The correction reaches a maximum of 9 per cent in M_NB and 3–5 per cent in other narrow bands, which we found in calibration data, rather than NGC 6302 data themselves. The calibration star is HR 7446, a B0.5III star, with magnitudes $L' = 5.055 \pm 0.010$ mag and $M = 4.996 \pm 0.040$ mag, respectively (van der Bliek, Manfroid & Bouchet 1996). Magnitudes for the narrow-band filters were derived by calculating colours for a 31 500 K black body to represent the B0III star (Tokunaga 1999). We assume that a 11 400 K black body (cf. van der Bliek et al. 1996) has colours of zero at all the bands. Including the effects of filter and atmospheric transmission (Lord 1992), we obtain NB_3.21 − L′ = −0.025, NB_3.28 − L′ = −0.017, L′ − NB_4.07 = −0.010 for a B0III star. We assumed that the magnitude of HR 7446 at M_NB is the same as that for the wide-band M. HR 7446 does not have strong hydrogen emission (Mennickent & Vogt 1988), but the assumption of a black body may produce a systematic error in the Brα calibration.

Aperture photometry for NGC 6302 is listed in Table 1, together with fluxes for zero magnitude ($F_{\nu 0}$ in Jy). The aperture is centred on RA = $17^{\rm h}13^{\rm m}44^{\rm s}.3$, Dec. = $-37°6'6''.4$(J2000) and has a radius of 13.5 arcsec. The errors are up to 20 per cent in M_NB, and about 10 per cent in the other filters.

We use the VLT optical image (ESO 1998) as a reference to find the alignment between the infrared images and the optical images. Two 2MASS stars are visible in both the infrared and optical VLT images 17134414−3706361 and 17134175−3706085. Fig. 4 shows that the brightest infrared source is coincident with the brightest position in the optical. The optical dark lane is still considerably fainter in the infrared.

2.2.1 *Brα and radio continuum*

Although the *HST* Hα traces the ionized gas, it is heavily affected by extinction. To measure the true distribution in the central region, infrared hydrogen lines, especially Brα, or radio free–free continuum should be used.

The Brα image (Fig. 5) is obtained from the NB_4.07 image, by subtracting a continuum image interpolated from the NB_3.21 and M_NB images in logarithm scale. The Brα intensity, measured through circular apertures of 3.2, 7.1, 10.6 arcsec radius, gives 1.6×10^{-11}, 4.8×10^{-11}, 5.0×10^{-11} erg cm^{-2} s^{-1}, respectively. Assuming that the NB_3.21 and M_NB bands have 10 per cent error and the M_NB may have up to 20 per cent, gives an uncertainty

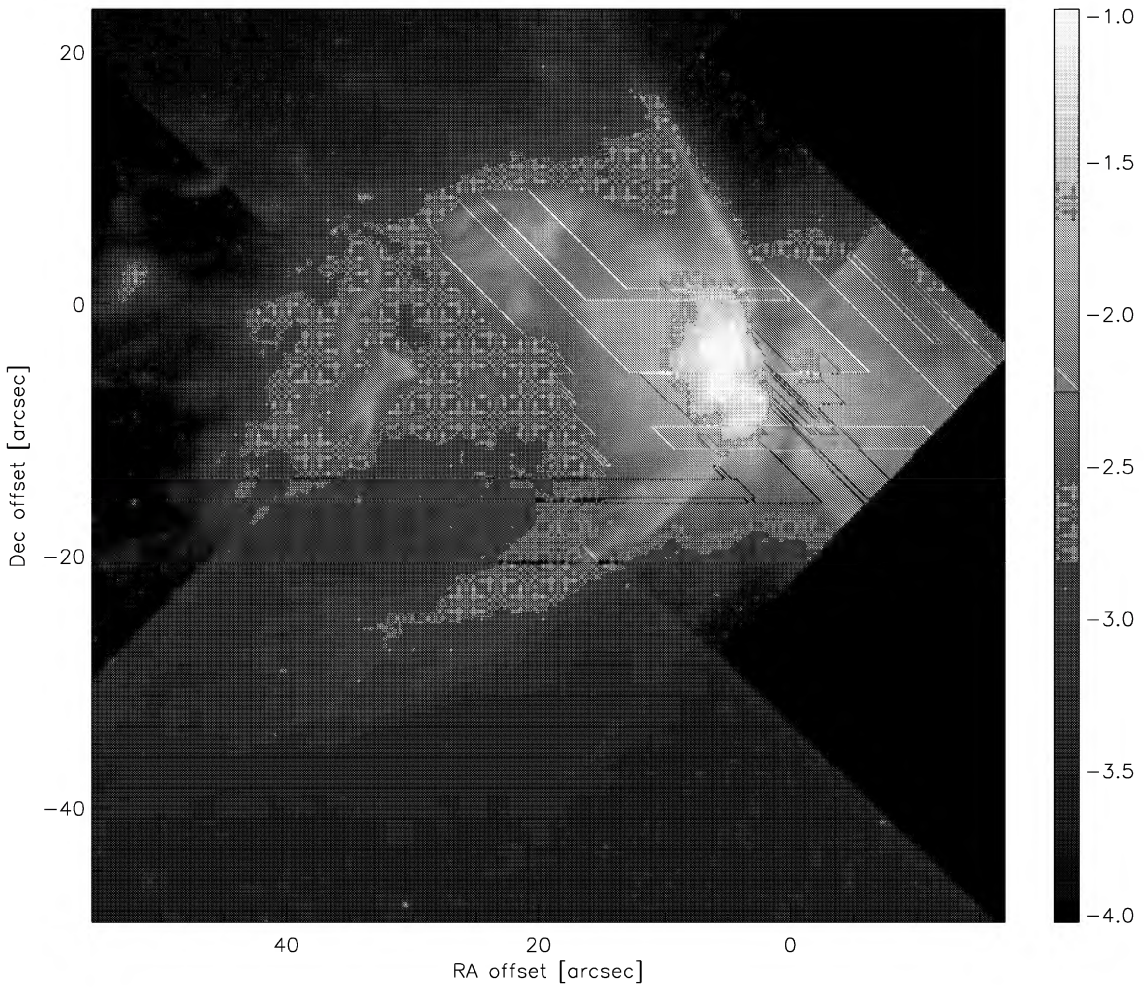

Figure 1. The *HST* WFPC2 image in the F656N band ($\lambda_0 = 6564$ Å, $\Delta\lambda_0 = 21.5$ Å) before the distortion correction. The scale is $\log I_\nu$ in Jy arcsec^{-2}. This image is dominated by the Hα line, with some contribution from [N II] lines and continuum. The reference position (RA offset, Dec. offset) = (0,0) is RA = $17^h13^m44\overset{s}{.}2$, Dec. = $-37°6'6\overset{''}{.}1$(J2000).

Table 1. Filters, image quality and fluxes. The central wavelengths (λ_0) and the widths of the filters are listed. $F_{\nu 0}$ is calculated flux at the zero magnitude, and F_ν is the flux of NGC 6302 through a 13.5 arcsec circular aperture centred on RA = $17^h13^m44\overset{s}{.}3$, Dec. = $-37°6'6\overset{''}{.}4$($J = 2000$)

Band	λ_0	$\Delta\lambda$	$F_{\nu 0}$	F_ν	FWHM	
					EW	NS
	(μm)	(μm)	(Jy)	(Jy)	(arcsec)	
M_NB	4.66	0.10	174.12	10.40	0.37	0.27
NB_3.21	3.21	0.05	343.40	1.95	0.37	0.43
NB_3.28	3.28	0.05	331.02	6.33	0.34	0.39
NB_4.07	4.07	0.07	223.85	10.29	0.28	0.31

of 25 per cent, or 0.3 mag. Beintema & Pottasch (1999) measured a Brα intensity of 1.538×10^{-11} erg cm^{-2} s^{-1}, using the 14 × 20 arcsec^2 *Infrared Space Observatory* Short Wavelength Spectrometer (ISO/SWS) aperture. They report that 50 per cent or more of the flux is missing because the ISO/SWS aperture is not large enough to cover the whole nebula. However, the large discrepancy with our values suggests that either the ISO aperture was not well centred on the nebula, or that our Brα flux is too high. If the latter is the case, the extinction at the wavelength of Brα, which we will discuss later, may be underestimated. Cassasus (private communication) measured 4.17×10^{-11} erg cm^{-2} s^{-1} with 3 × 3 arcsec^2 slit. This suggests with 3.2 arcsec radius, Brα intensity is about 1.5×10^{-11} erg cm^{-2} s^{-1}. This is consistent with our measurement, and Brα intensity in Beintema & Pottasch (1999) may be underestimated.

At RA offset= +2 to 3 and Dec. offset= −4 to −6, the Brα intensity becomes negative (from −0.01 to −0.03 Jy arcsec^{-2}) after continuum subtraction. (In Fig. 5, this region is blacked out because of the logarithmic scale used.) The value in this negative region is about 10 per cent of M_NB and is within our uncertainties.

Gómez et al. (1989) present a 6-cm continuum map, obtained with the Very Large Array (VLA) observations taken 1987 July 14. We retrieved the data from the VLA archive. The data were reduced using the AIPS package, using uniform weighting in the UV plane. The beam size is 1.05 × 0.25 arcsec^2, with a position angle of 5 degrees. The cleaned image is shown overlaid on the Brα image in the bottom panel of Fig. 5. We aligned the 6-cm image with the Hα and Brα images so that the arc (cf. Fig. 8), and flares ([RA offset, Dec. offset]∼[4, −3], [2.5, −2] and [−2, −3]) coincide. The brightest spots in Hα, Brα and 6 cm

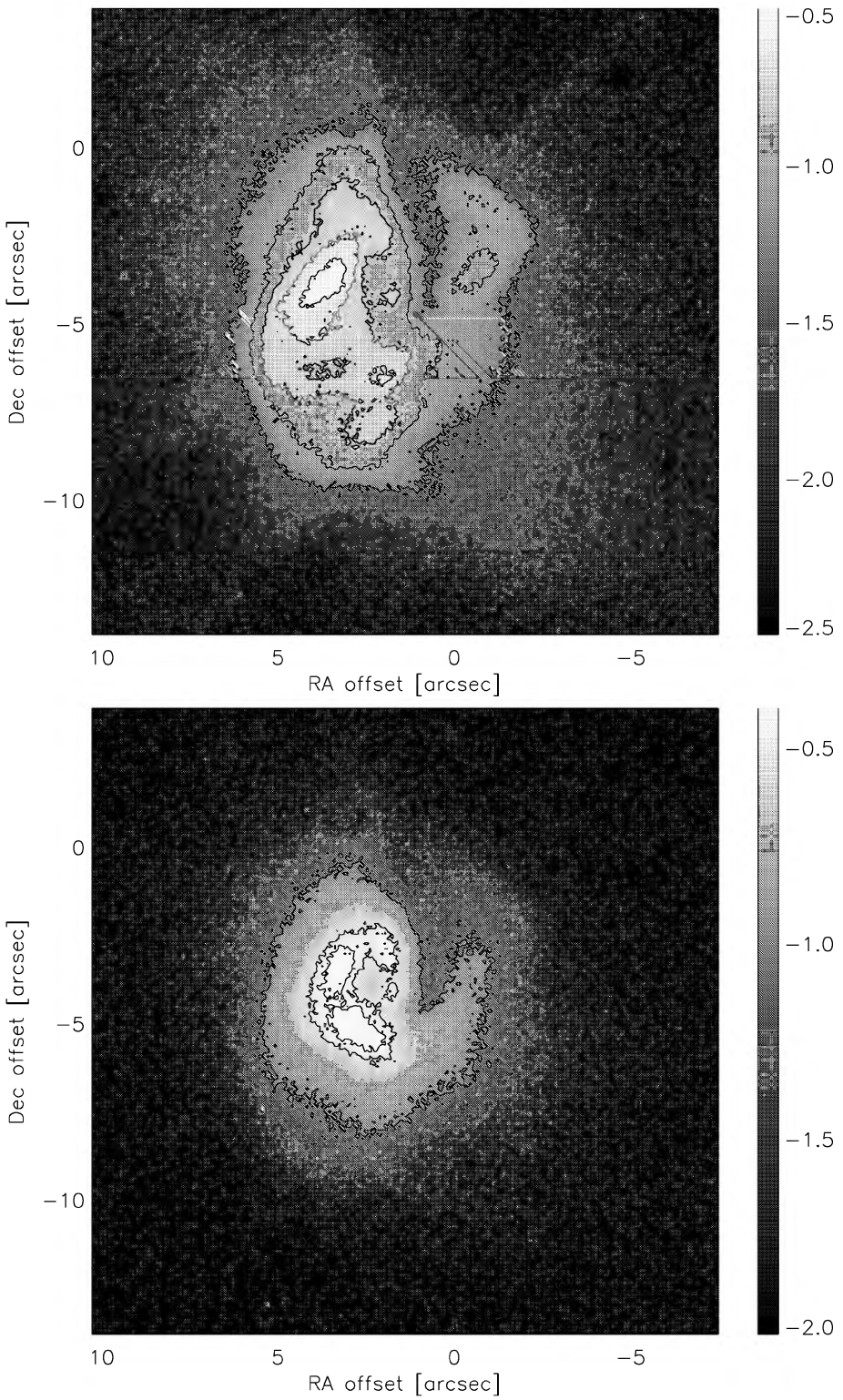

Figure 2. The NB_4.07 image, which represents Brα (top) and its nearest continuum, M_NB (bottom). The scale is log I_ν in Jy arcsec^{-2}. Contour lines show 0.05, 0.1, 0.15, 0.2, 0.25 Jy arcsec^{-2} in the NB_4.07 image, and 0.1, 0.3, 0.35 in the M_NB image.

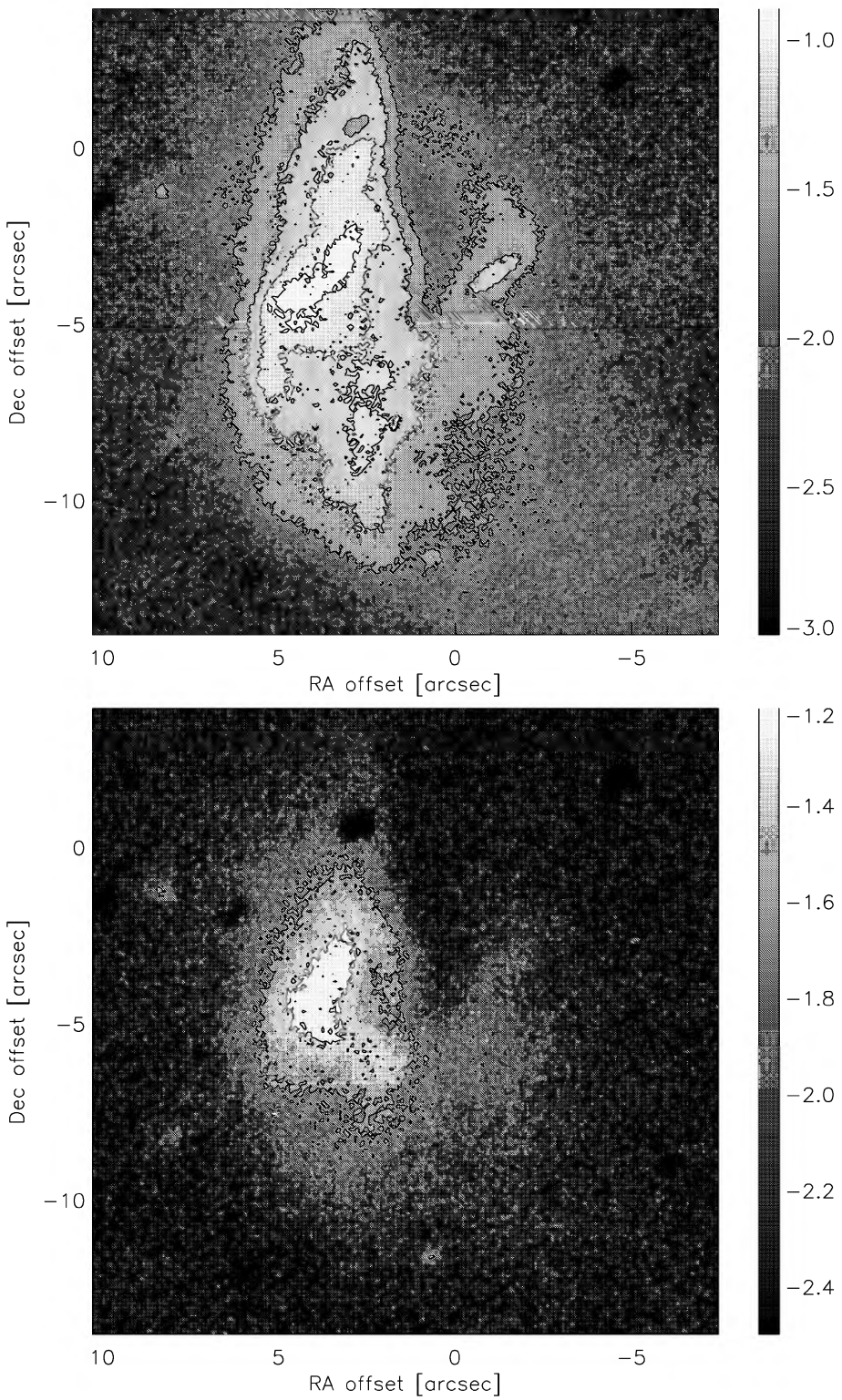

Figure 3. The NB_3.28 image (top) and its continuum band NB_3.21 (bottom). The scale is in log I_ν in Jy arcsec^{-2}. Dark spots at [RA offset, Dec. offset] = [−5, 3], [3, 1], [6, −2] and [9,2] are negative images of nearby stars, owing to chopping and nodding. Contour lines show 0.025, 0.05, 0.075, 0.1 Jy arcsec^{-2} in the NB_3.28 image and 0.025, 0.05 Jy arcsec^{-2} in the NB_3.21 image.

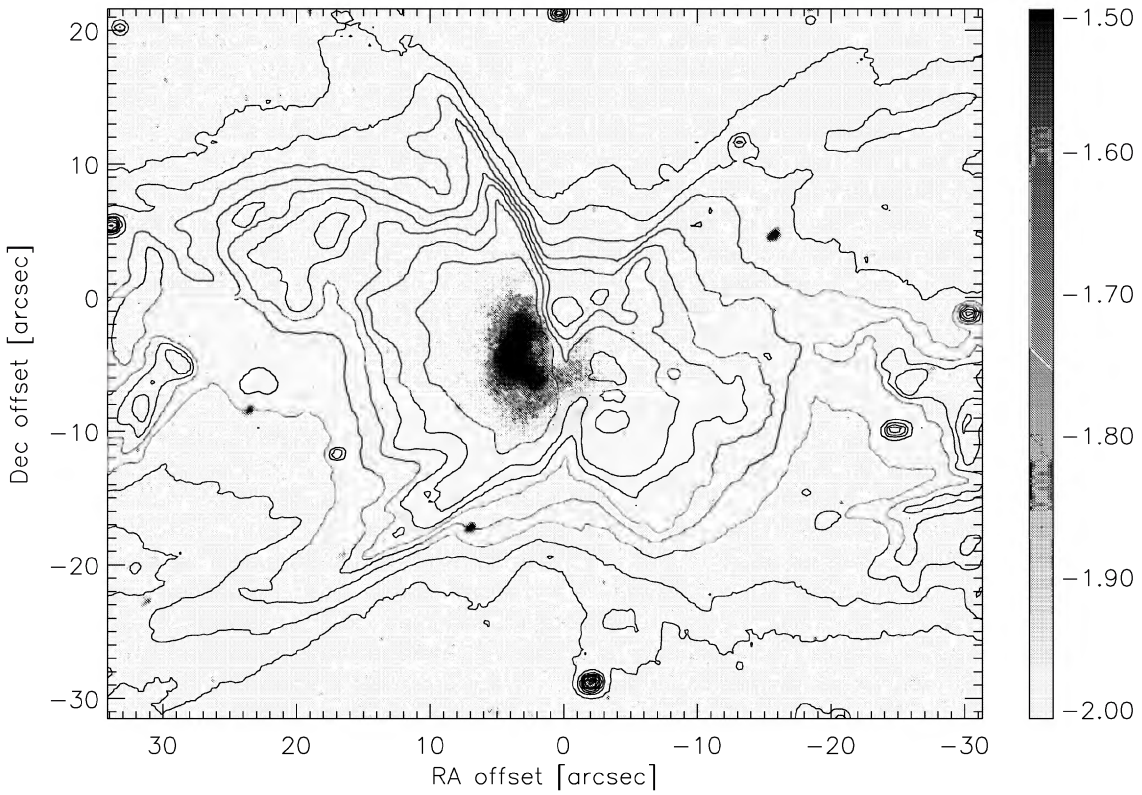

Figure 4. The ISAAC/VLT NB_3.21 image (in log I_ν in Jy arcsec^{-2}), with superposed the contours of an VLT optical RGB composite image (ESO 1998). (The RGB composite does not show physical values; inside the east lobe the VLT optical image is saturated.) The brightest infrared source is located within the optical east lobe, and not at the optical dark lane.

coincide inside the east lobe. The accuracy of the alignment is about half of the beam size of 6 cm image.

2.3 The James Clark Maxwell Telescope (JCMT) submillimetre image

NGC 6302 was observed with SCUBA/JCMT (Holland et al. 1999) on 1998 April 15. Two band (narrow band 450- and 850-μm bands) images were obtained simultaneously. The background was subtracted with chopping by 120 arcsec in longitude. The object was observed in 'jiggle map mode', and several images with slightly different positions were co-added. The atmospheric opacity (τ), derived from the measured τ at 225 GHz,[1] is $\tau = 0.12$ at 850 μm, and 0.50–0.52 at 450 μm. The beam widths are approximately 7 arcsec at 450 μm and 13 arcsec at 850 μm. The data were reduced with the STARLINK SOFTWARE ORAC-DR and SURF. We cannot accurately align the JCMT data to other data. The position of Fig. 6 is based on the FITS header, and not corrected to fit with the ISAAC data. The SCUBA 450-μm image (which has better resolution) is shown in Fig. 6. It shows a core of emission with wings extending east–west.

The flux conversion factors (volts to Jy per beam) were obtained by the observatory only for point sources (855 and 248 Jy per beam per volt at 450 and 850 μm, respectively). These conversion factors applied to the peak fluxes, yield 38.9 Jy at 450 μm and 5.8 Jy at 850 μm. Owing to the uncertainty of atmospheric opacity, and flux conversion factors, the flux accuracy may be as much as 50 per cent in error. Assuming that the beam is approximately Gaussian, about 55 per cent of the flux comes from the lobes, although the point-spread function is not accurately known.

The total extended 450-μm flux is given by Hoare, Roche & Clegg (1992) as 46 Jy at 350 μm, and 3.82 Jy at 800 μm. According to spectra in Hoare et al. (1992), about 90 per cent of the flux at 450 μm is dust emission, while the remaining 10 per cent is free–free emission from the ionized gas. This ratio, compared to the fact that about half the 450-μm flux comes from the wings, shows that in the wings the emission is mostly owing to dust. We confirm this by extrapolation from the 6-cm map. The brightest region in the 6-cm map shows a flux of the order of 2×10^{-2} Jy arcsec^{-2}. This gives a hydrogen free–free continuum emission at 450 μm of 0.4 Jy per beam at 450 μm, assuming the electron temperature is 1.8×10^4 K and the electron density is 10^4 cm^{-3}. The brightest region at 450 μm has a peak flux density of more than 3 Jy per beam. The wings have a 6-cm flux less than 0.0025 Jy arcsec^{-2}, which predicts less than 0.5 Jy per beam at 450 μm. The 450-μm flux is less than 1 Jy per beam in the lobes. This extrapolation is not conclusive for the wings.

3 IONIZED GAS – KNOTS AND CLUMPS

Fig. 7 shows the large-scale structures of the NGC 6302 optical image. There are clear edges in the outflows towards the north–north-east and south-east. There is another outflow towards north-east; cirrus structure is found inside this outflow, suggesting the presence of turbulence within the wind. The outer, low-excitation region of NGC 6302 shows several clumps and knots. All three knots show

[1] http://docs.jach.hawaii.edu/JCMT/SCD/SN/002.2/node5.html

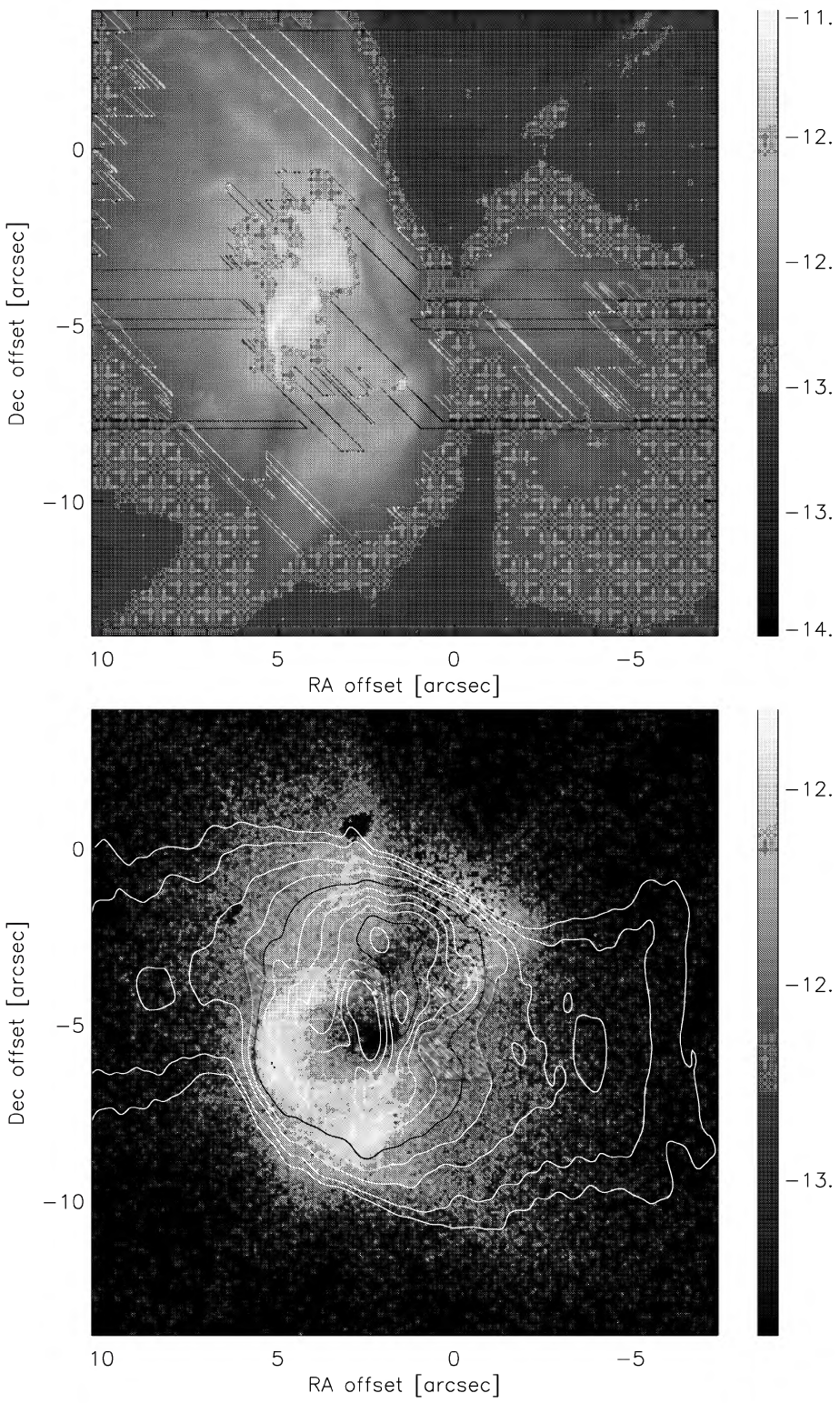

Figure 5. (Top) The central region of the Hα image taken by *HST*. The scale is log I_ν in erg cm^{-2} s^{-1} arcsec^{-2} units. (Bottom: grey-scale) The Brα (NB_4.07) image after continuum subtraction. The scale is log I_ν in erg cm^{-2} s^{-1} arcsec^{-2} units. (Bottom: contour) The radio 6-cm continuum contours. The peak is 0.0479 Jy arcsec^{-2}. Contour lines are 0.0025, 0.005–0.045 Jy arcsec^{-2} with 0.005 Jy arcsec^{-2} grid, and 0.02 and 0.04 Jy arcsec^{-2} lines are shown in black.

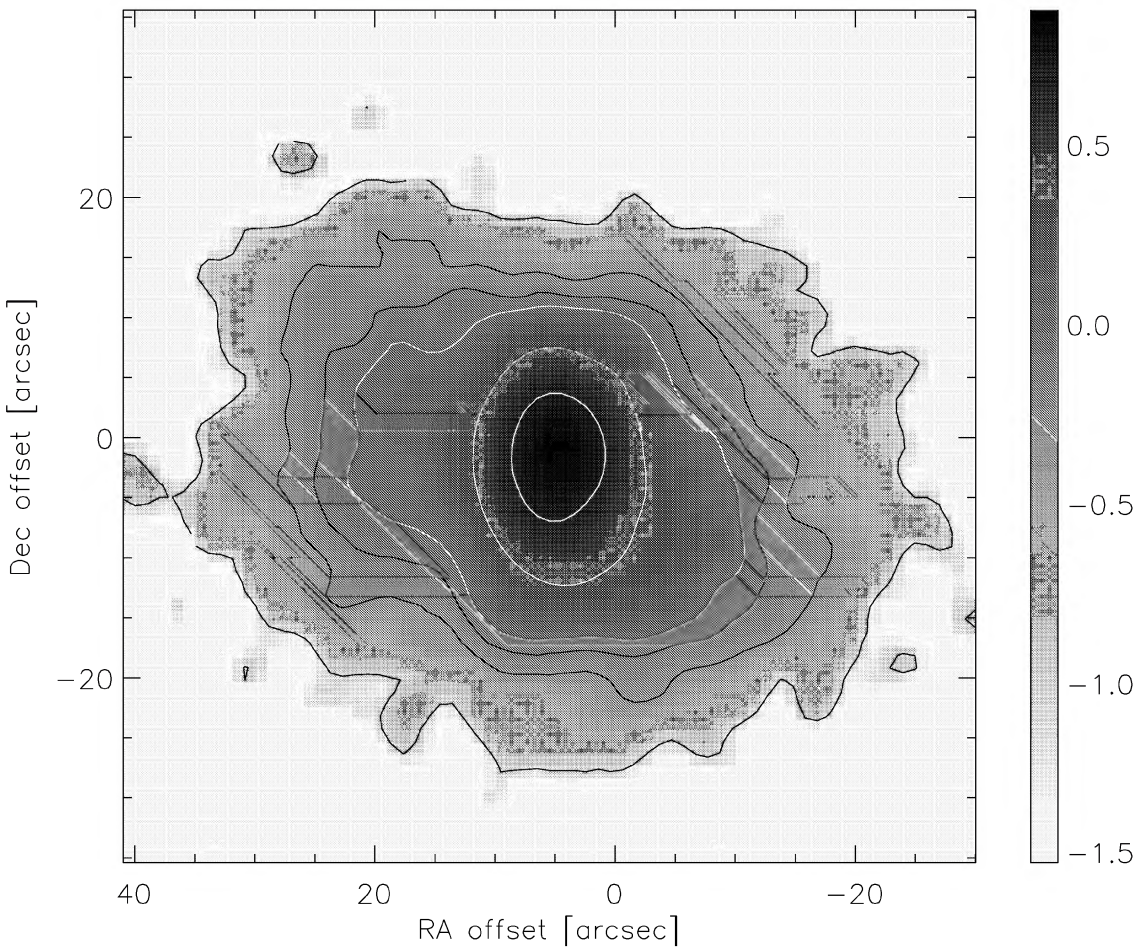

Figure 6. The SCUBA/JCMT 450-μm image in log I_ν in Jy per beam. The contour levels are 0.1, 0.5, 0.75, 1.0, 2.5, 5.0 Jy per beam. The position is according to the observatory information, and is not otherwise registered.

the wind tail to the east, pointing away from the star. Such knots are also found in the elliptical PN, NGC 2392 (O'Dell et al. 2002). Their origin could be either primordial or instability related (e.g. López-Martín et al. 2001). The largest clumps are rather 'wall' like, indicative of gas compressed by the fast wind. Even further east, additional knots and clumps are found.

The central region shows evidence for interactions between the fast stellar wind and the dense gas, resulting in thin shock fronts. There is a knot in the central region (Fig. 8), which is located at the tail of a filament pointing *towards* the star. This knot appears to be accelerated by the fast wind. This type of knot is found in the proto-PN Frosty Leo (Sahai et al. 2000, the knot is on the far side of the central star of jets (J1) and (J3)). An arc in the Hα image coincides with the radio shell: its structure suggests the presence of a hot bubble in the cavity within the radio shell. The outflows show filament-like structures, suggesting discontinuous mass loss or interaction of the fast wind with the dense gas.

Evidence for a fast wind in NGC 6302 was found by Meaburn & Walsh (1980), who found wings on the [Ne v] line extending to 500 km s^{-1}. Similar velocities are found by Feibelman (2001, 520 km s^{-1} on the C iv 1546-Å line) and Gómez et al. (1989, 300 km s^{-1} width of the radio recombination line). However, Cassasus (private communication) has not been able to confirm the [Ne v] wings, and suggest these data may contain an instrumental artifact. All models for the evolution of polar flows require fast winds at some phase of the stellar evolution. Lack of evidence for a current fast wind would not contradict these models, but would imply the presence of such a wind in the past.

4 DUST DISTRIBUTION

4.1 Extinction maps

The Hα is strongly affected by the extinction. The Brα is less affected but still shows distinct suppression at the location of the dark lane. The radio emission is unaffected. This allows us to map the extinction across the source, and to image the structure of the lane by the extinction variations.

We derive the extinction map of NGC 6302 from the ratio of the Brα or Hα with the 6-cm continuum data of Gómez et al. (1989). We use the *HST* image (Fig. 5) directly as the Hα flux, as the continuum contribution is minor. The Hα and Brα images are smoothed to the spatial resolution of the 6-cm image. The Hα image gives accurate extinction in regions of lower extinction, but saturates in the dark lane. Brα is the best tracer for the dark lane. The Brα is affected by a systematic uncertainty (Section 2.2.1), but this does not affect the structures seen.

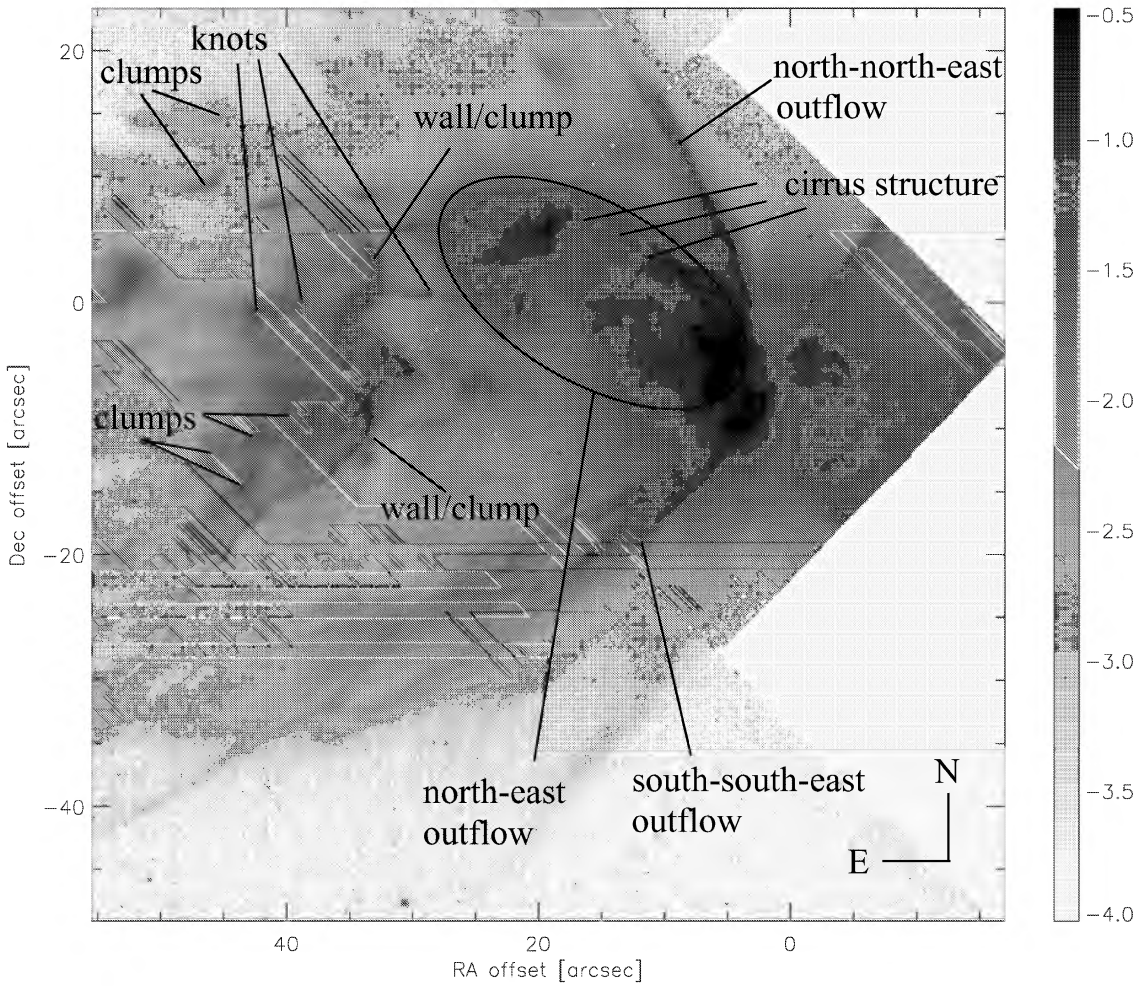

Figure 7. Schematic view of outer region of NGC 6302 overlaid on the *HST* F658N image, which shows more complicated structure than the Hα image. The surface density is calibrated as log F_ν in Jy arcsec^{-2}.

The extinction is estimated following Milne & Aller (1975) under the assumption of case B. The effective coefficient for Hβ is taken from Kwok (2000), and the effective ratio of Brα or Hα to Hβ are taken from Hummer & Storey (1987), Hummer & Storey (1995). We adopt $T_e = 1.8 \times 10^4$ K and electron density $N_e = 10^4$ cm^{-3}, as given in Milne & Aller (1975).

The extinction maps are shown in Fig. 9, and values of $A_{Br\alpha}$ and $A_{H\alpha}$, at representative places (mostly local maxima or minima) are summarized in Table 2.

The interstellar extinction is unknown. Two nearby stars (HD 155464 and HD 155364), which are approximately located at 843 and 626 pc, respectively estimated from V magnitudes and spectral type, suggest $dE(B-V)/ds = 0.34$ mag kpc^{-1}, and $A(V) = 1.1$ mag and we take this as the interstellar extinction. For the hydrogen recombination lines, assuming a galactic interstellar extinction law (Cardelli, Clayton & Mathis 1989), $A_{H\alpha} = 0.91$ mag and $A_{Br\alpha} = 0.05$ mag is derived.

The dark lane shows a significant north–south extinction gradient, with the highest values found to the north of the ionized inner shell. The peak is consistent with a torus or ring, showing the highest column density at the tangential point. There is no clear opposite peak, but a weak possible one is located at (RA offset, Dec. offset)=(0,−8), due south of the northern peak. There is an intrinsic asymmetry in the obscuring structure. The radio torus also shows a lower intensity in the south, indicating a lower density.

At the higher resolution of *HST*, a secondary, thin extinction lane is seen 1-arcsec east of the main lane. This feature is lost in the extinction maps because of the required smoothing. The double lanes, oriented at different angles, is a unique feature among PNe.

The wings also show different extinction peaks. Two symmetrically opposed peaks are seen at 5 arcsec from the centre, and a further peak at 10 arcsec.

The Brα extinction shows a central minimum, owing to the lack of Brα emission at that point. In the colour map, a thin shell of lower extinction is seen towards the south [e.g. at (RA offset, Dec. offset)=(5, −7)], which corresponds to a feature in the *HST* image, at the outer rim of the radio torus.

Casassus, Roche & Barlow (2000) estimate $A_V = 3.7$ mag averaged over a 3 × 3 arcsec^2 aperture. Pottasch et al. (1996) report $E(B-V) = 0.855$ mag based on various methods, weighted towards the brightest region and this is equivalent with $A_V = 2.8$ mag if $R(V) = A(V)/[A(B) - A(V)] = 3.1$ mag (Mathis 1999). Bohigas (1994) reported $C(H\beta)$=1.56 at the brightest location (equivalent

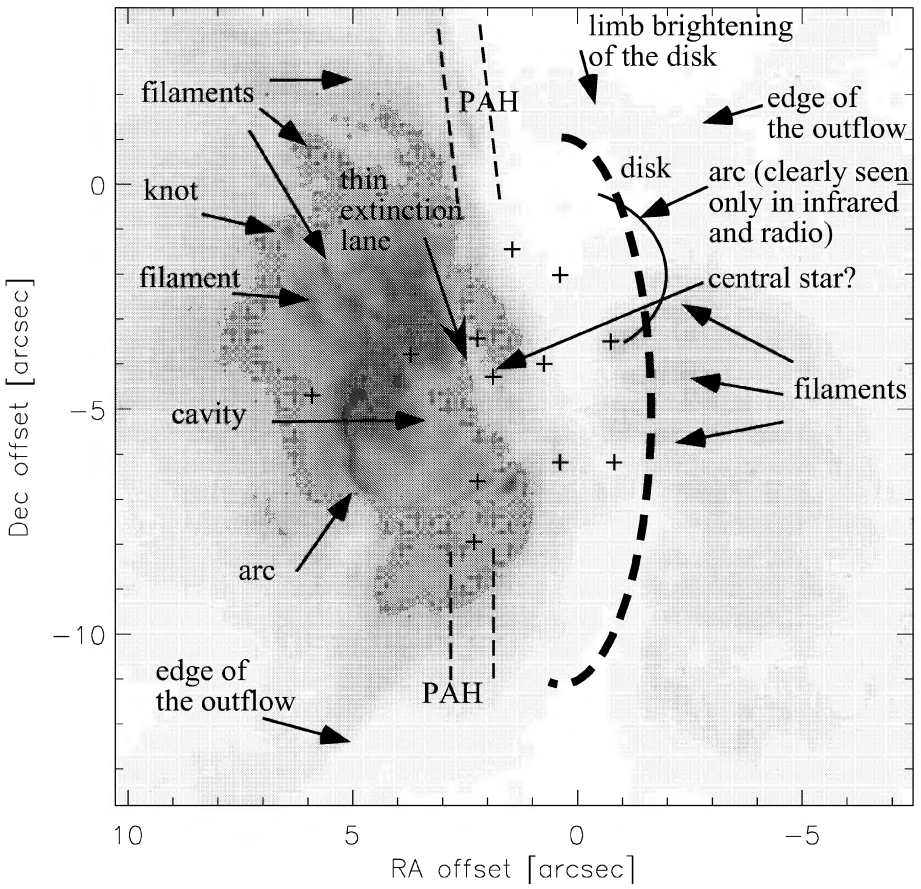

Figure 8. Schematic view of central part of NGC 6302 overlaid on the *HST* Hα image. The structures seen in this image are shown with solid lines, and those seen in other bands are shown in dashed lines. Crosses show the locations where Hα and Brα fluxes are listed in Table 2 (see also Fig. 9).

with $A_V = 3.35$ mag). Our results show $A_{\mathrm{H}\alpha}$ of 3.46 mag (equivalent with $A_V = 4.24$ mag) and 3.77 mag (equivalent with $A_V = 4.61$ mag) at the bright regions (a) and (b). The slightly higher values are probably owing to the higher spatial resolution. The highest values at the dark lane exceed $A_{\mathrm{Br}\alpha} > 1.0$ mag and $A_{\mathrm{H}\alpha} > 6.0$ mag, at regions (h), and (m) (Fig. 9 and Table 2).

4.2 Difference in Hα and Brα

There are clear differences between the Hα and Brα images, which also are seen in the Hα and Brα extinction maps. For example, at (RA offset, Dec. offset)=(1, −2) in Fig. 5, there is an arc structure in the Brα and 6-cm images, but this arc is not found in the Hα image. This region also shows different structure in the extinction maps Fig. 9(g). There is a flux cavity in the Brα image. The reality of the cavity is indicated by the 6-cm radio continuum which shows similar structure to the Brα image. In addition, the cavity is already found in the images NB_4.07 and NB_3.28 before the continuum subtraction.

The southern part of the cavity is seen in the optical (Hα), but arc structure in the north is hidden by the high extinction of the dust lane.

Any gas located inside the cavity must emit little free–free and hydrogen recombination emission. Several PNe are known to contain a hot bubble in their central cavity, caused by the shocked fast wind from the central star. Temperatures of this bubble are $\sim 10^6$ K; the gas is detected by thermal X-ray emission (Kastner et al. 2002). Gas at such temperatures emits little optical and radio emission. Evidence for such bubbles may also come from acceleration seen at the inner edge of some PN (Gesicki & Zijlstra 2003). The cavity in NGC 6302 may therefore not be empty but could be filled with such a low-density, hot gas.

The highest extinction at Brα is 2 mag, which corresponds to more than 30 mag in Hα, assuming a normal interstellar extinction curves. However, measured extinction at Hα is only 6 mag. The discrepancy may be attributed to 'grey' extinction, indicative of large dust grains. Such a grey extinction has been suggested in other PNe and post-AGB stars (Waelkens et al. 1992; Pottasch, Beintema & Feibelman 2000). However, another plausible explanation is that the dust layer is embedded within the ionized structures. In this case, the gas behind the extinction layer shows the full extinction, but the flux also contains a small component from the front layer, with much lower extinction. In this situation, the measured extinction at shorter wavelengths (compared to radio) will asymptotically approach a limit given by the fraction of gas located in front of the layer.

4.3 PAH distribution

The analysis of ionized gas shows NGC 6302 is oxygen rich (Beintema & Pottasch 1999). The oxygen-rich nature of the disc is confirmed by the presence of OH emission (Payne, Phillips & Terzian 1988). However, the fact that PAH emission is also found in NGC 6302 (Roche & Aitken 1986) shows that some carbon-rich

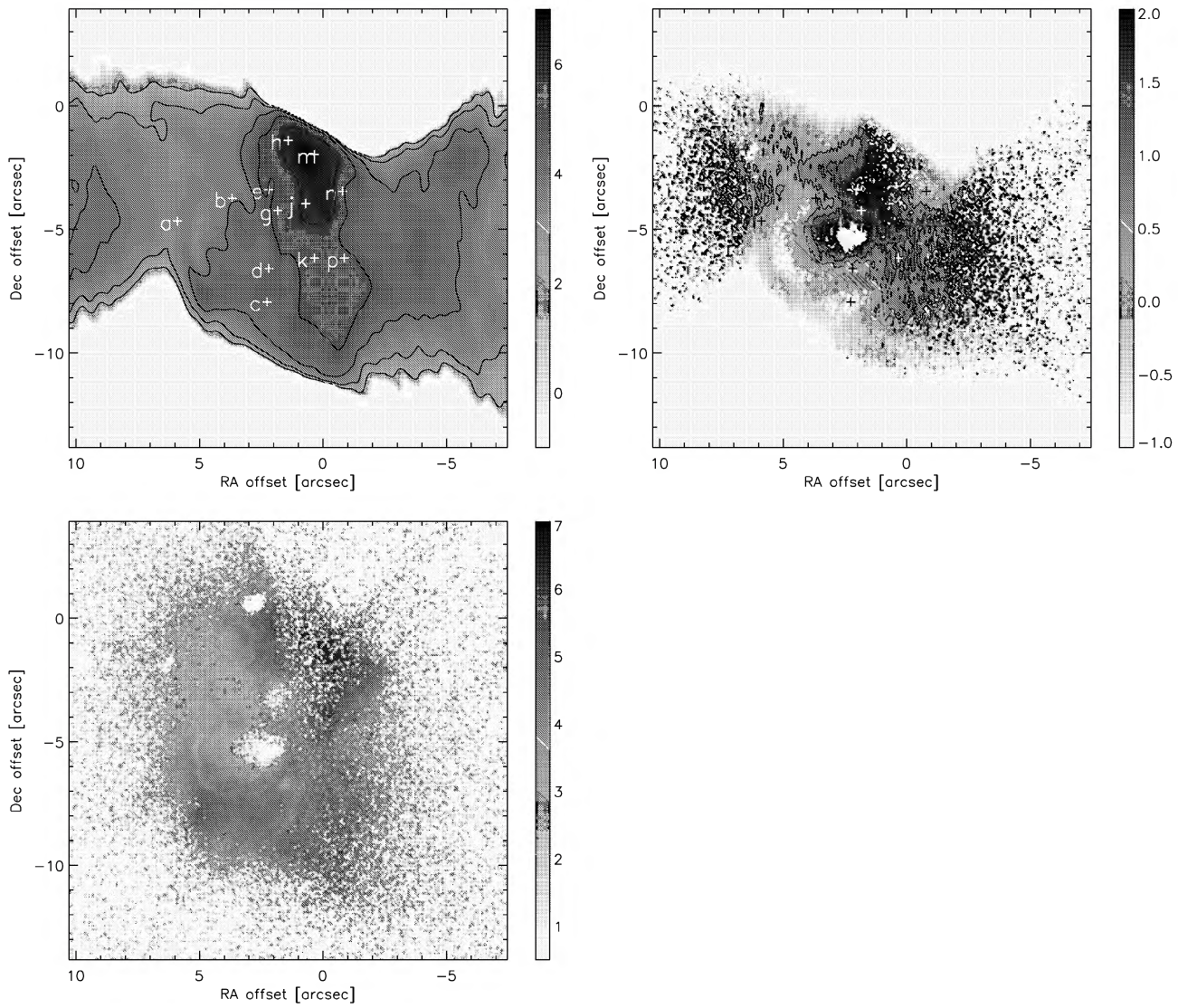

Figure 9. Extinction maps derived from and Hα and 6 cm (top left), Brα and 6 cm (top right), and the colour excess $E(\mathrm{H}\alpha - \mathrm{Br}\alpha)$ (lower left) in magnitudes. Crosses show the positions for which extinction is summarized in Table 2. The grey-scale coding for the extinction is shown in the vertical bars; the contour levels are at: 2, 3, 4, 5, 6 mag (Hα image); 0.5, 1.5 mag (Brα image).

Table 2. The extinction measured at various locations. $I_{\mathrm{Br}\alpha}$ and $I_{\mathrm{H}\alpha}$ are in units of log(erg cm^{-2} s^{-1} arcsec^{-2}). The 6-cm intensity ($I_{\nu=6\,\mathrm{cm}}$) is in units of Jy arcsec^{-2}. The values are not corrected for interstellar extinction, estimated as $A_{\mathrm{H}\alpha} = 0.91$ and $A_{\mathrm{Br}\alpha} = 0.05$ mag.

	Position (arcsec)	(arcsec)	$I(\mathrm{Br}\alpha)$	$I(\mathrm{H}\alpha)$	$I(\nu = 6\,\mathrm{cm}) \times 10^{-2}$	$A(\mathrm{Br}\alpha)$ (mag)	$A(\mathrm{H}\alpha)$ (mag)	$E(\mathrm{H}\alpha - \mathrm{Br}\alpha)$ (mag)
a	5.89	−4.69	−12.39	−12.27	1.20	0.03	3.46	3.61
b	3.69	−3.76	−12.04	−11.88	3.64	0.40	3.85	3.52
c	2.27	−7.95	−11.85	−12.22	2.84		4.43	
d	2.20	−6.60	−12.05	−12.12	3.43	0.24	4.45	4.08
e	2.20	−3.41	−12.61	−12.34	3.65	2.78	4.99	3.20
g	1.85	−4.26	−12.33	−12.39	3.89	1.34	5.25	4.04
h	1.42	−1.42	−12.70	−13.07	2.67	1.74	6.36	4.83
j	0.71	−3.98	−12.69	−12.86	3.47	2.17	6.17	4.34
k	0.35	−6.18	−12.52	−12.61	2.19	1.19	5.26	4.11
m	0.35	−1.99	−12.49	−13.23	2.81	1.24	6.83	5.75
n	−0.78	−3.48	−12.02	−12.56	2.14	−0.19	5.15	5.25
p	−0.85	−6.18	−12.75	−12.87	1.52	0.72	5.30	4.19

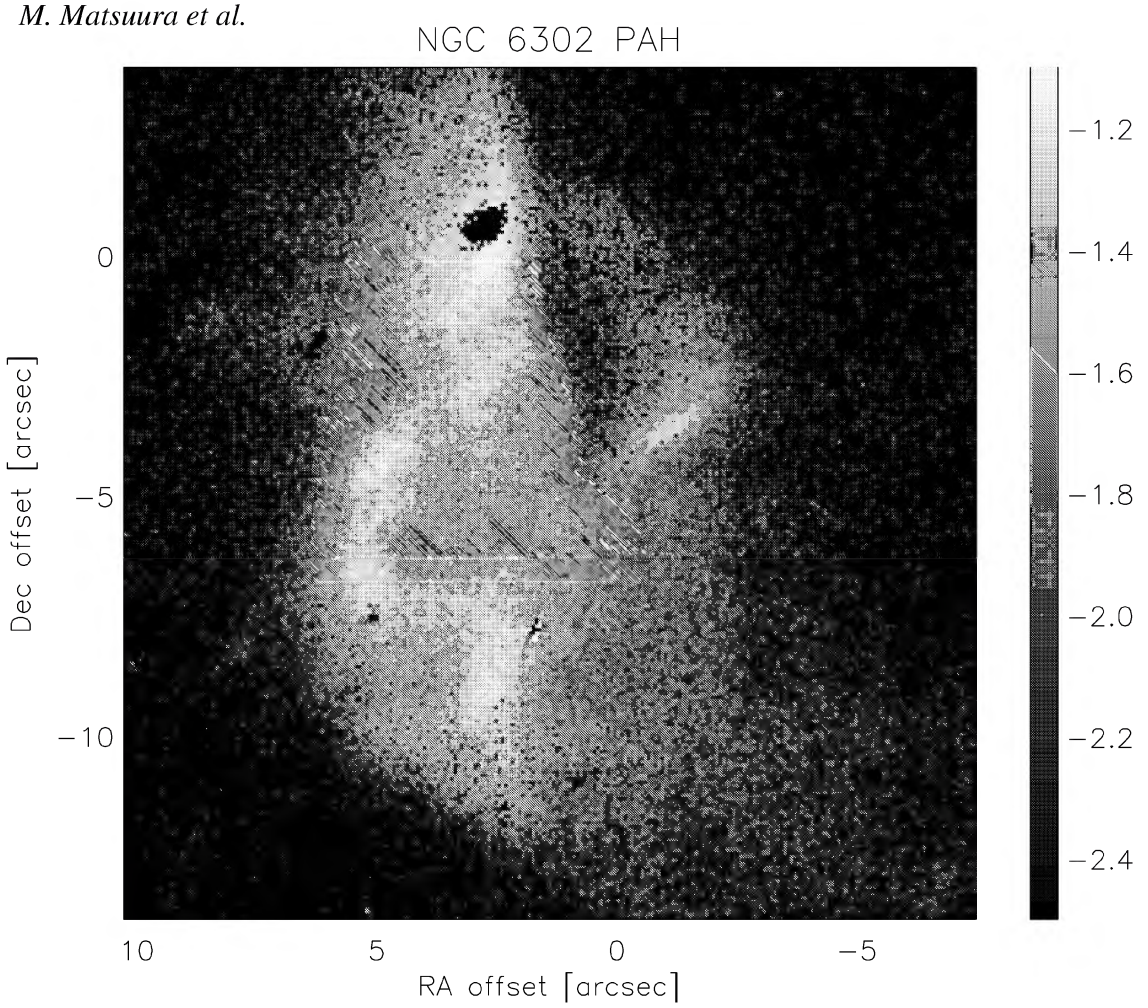

Figure 10. The PAH image of the core region. The colour is log I_ν in Jy arcsec^{-2}.

material is also present. This dual chemistry is rare in post-AGB objects, and appears to be seen in bipolar nebulae only (Molster et al. 1999). PAH emission requires excitation by UV and/or optical photons which do not penetrate the dark lane. The PAH emission is therefore located either near the surface of the disc, or in the (irradiated) outflow.

The distribution of the PAH emission is shown in Fig. 10, obtained by subtracting the continuum image (NB_3.21) from the image of NB_3.28. The *L*-band spectra (Casassus et al. 2000) show some contamination by the Pfδ + He I 6–7 line in NB_3.28. This helium line contributes 20–30 per cent of the continuum-subtracted intensity in NB_3.28 in the central 3 × 3 arcsec^{-2} region (Casassus et al. 2000). We argue that the 3.3 μm shows mainly PAH, based on the similarity between the 11.3-μm PAH image (Kemper et al. 2002) and our 3.3-μm image.

The PAH distribution is similar to that of the ionized cavity. No clear PAH emission is found in the dark lane, but a local peak is present near the northern spur. In this region, the PAH emission is more extended than Brα (Fig. 11). In the east–west direction, the PAH emission peaks at a similar location as the Brα.

In ionization-bounded nebulae, the PAH distribution tends to be more extended than that of the ionized gas [e.g NGC 7027: Woodward et al. (1989); the Orion bar: Sellgren, Tokunaga & Nakada (1990)]. Omont (1986) concludes that strong UV radiation from the central star destroys PAHs in the ionized region. For NGC 6302, the PAH distribution suggests that the ionized core region is ionization bounded in the north–south direction but density bounded east–west.

Fig. 12 shows the entire NB_3.28 VLT image. This band shows a very faint shell located 25 arcsec to the northeast. No other infrared band shows emission this far out, although the sensitivity of NB_3.21 and NB_3.28 should be similar. This distant emission can be either PAH or He I, although the fact that no other such structure is seen argues against the latter.

5 DISC PROPERTIES

5.1 SED model fit

The dust mass can be derived by fitting the spectral energy distribution (SED). We consider heating of the dust by the central star, using the radiative transfer code of Nomura (2002) and Nomura & Millar (2004). The radiative transfer is solved assuming spherical symmetry. As long as the disc is edge-on, i.e. the central star is not directly seen, this assumption will not cause a significant discrepancy in the calculated SED. A detached dust shell is assumed with a inner and

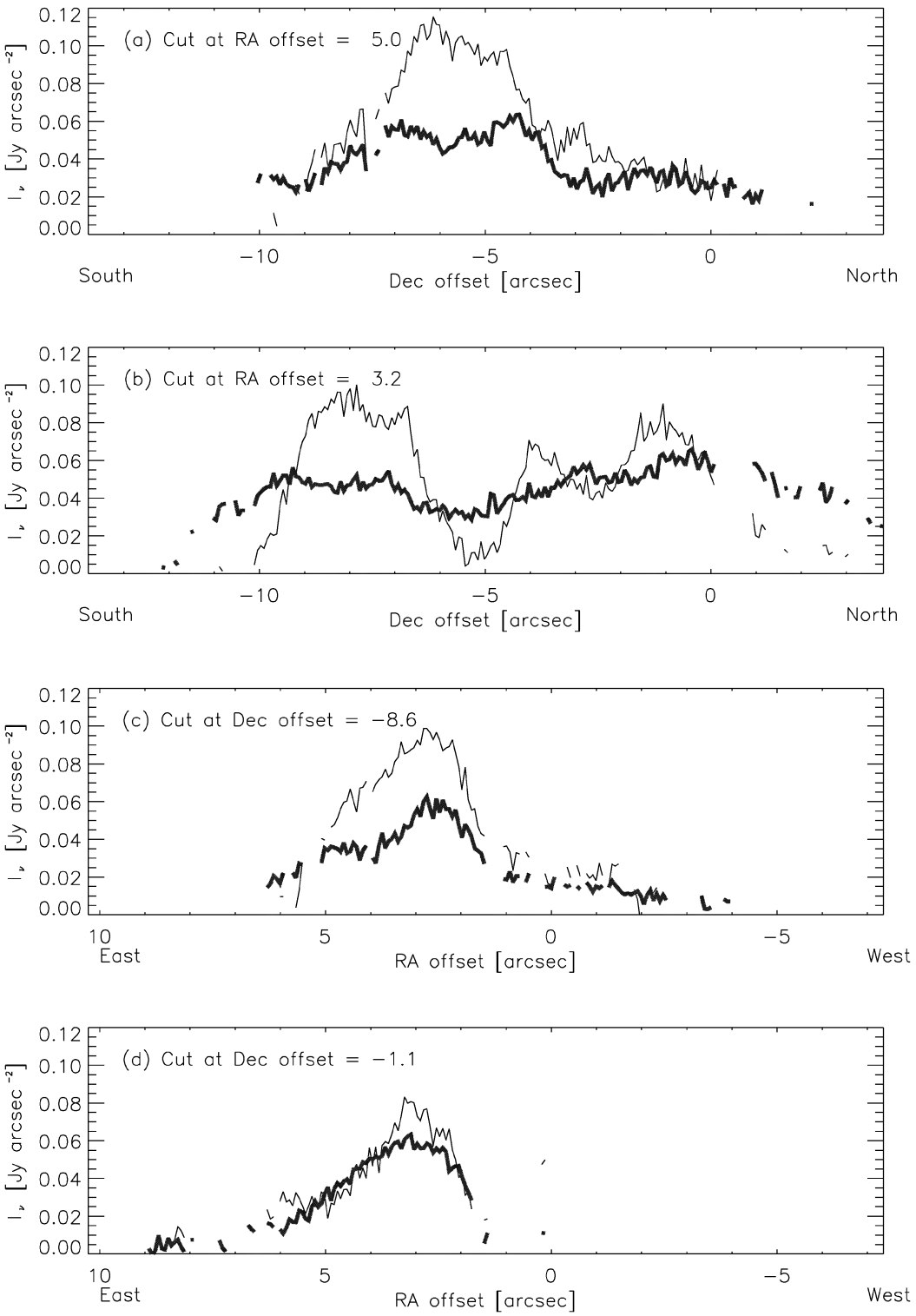

Figure 11. PAH distributions (grey thick lines) along the north to south directions at RA offset = 5.0 arcsec (a) and at RA offset = 3.2 arcsec (b). For comparison, the Brα distributions are shown in thin black lines. Surface density is averaged over the neighbouring 5 pixels with the same Dec. coordinates. Panels (c) and (d) are the ones along the east to west directions.

an outer radius, $r_{\rm in}$ and $r_{\rm out}$. Two different radial distributions of dust grains are used: $\rho = \rho_0(r/r_0)^{-1}$ and $\rho = \rho_0(r/r_0)^{-2}$, where ρ is the dust density, and r is the radius, and subscript zero shows the values at the inner radius. The absorption coefficients of interstellar dust of Adams & Shu (1985, 1986) are used. The distance is taken as 1 kpc, and the luminosity as 2436 $L_\odot$ (obtained from the *IRAS* data). The temperature of the central star is assumed to be 1×10^5 K.

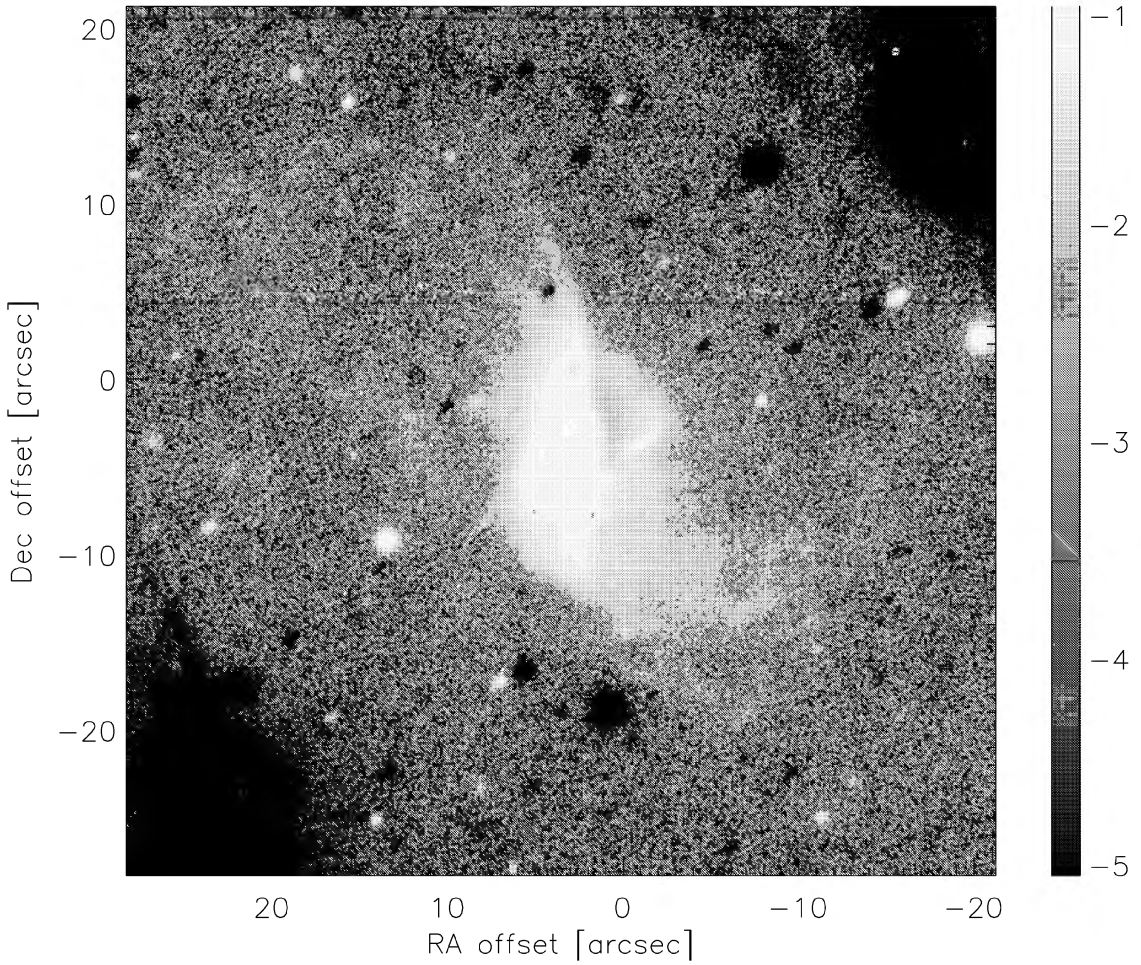

Figure 12. ISAAC/VLT image of NGC 6302 in NB_3.28. The faint shell in the north-east is seen only at NB_3.28, and not in other infrared bands, suggesting the excitation of PAH at about 25 arcsec away from the central stars. The colour is $\log I_\nu$ in Jy arcsec^{-2}. The negative images of chopping are located at the corners of north-west and south-east and at small bobs. Note that some of the stars in the images (both positive and negative) are artificial images created by shift-and-add of the chop-and-nodded images.

The observed fluxes are obtained from our work (the flux from the central region is used for the JCMT data), Hoare et al. (1992) and Milne & Aller (1982). The data and the fit are shown in Fig. 13(a). The free–free emission of hydrogen is scaled to the 6-cm flux: its contribution is negligible at infrared and submillimetre wavelengths, except at 800 μm. Little difference is found in the calculated SEDs from the two density profiles. The long-wavelength SED is fitted well with the model parameters $r_{\rm in} = 1 \times 10^{16}$ cm, $r_{\rm out} = 1 \times 10^{17}$ cm, and a dust mass of 0.03 $M_\odot$. The dust temperature ranges between 50 and 100 K (Fig. 13c).

Below 12 μm, the observed flux is much higher than the model fit, showing that a dust component with a much higher temperature must be present (Kemper et al. 2002). The near-infrared flux in the model could be increased if the disc is inclined so that the hot inner region is seen directly: the near-infrared flux is sensitive to both the inner radius of the disc, and to the inclination of the disc (e.g. Lopez et al. 1997). However, hot dust could also be located in the bipolar outflow. Especially, very small grains, which are easily heated by single photon capture, could increase the near-infrared without increasing the total mass significantly (Siebenmorgen, Zijlstra & Krügel 1994). Therefore, we do not aim to fit the hot component. Ignoring the hot component will not change the total mass drastically.

The model intensity profile is found in Fig. 13(b). The profiles are smoothed with the JCMT beam (Hogerheijde & Sandell 2000), and compared with the observed profile (Fig. 13d). The calculated north–south profile reasonably traces the observed one. The radial intensity profile is fitted better with the r^{-1} density distribution. χ^2 is 34 and 53 for r^{-1} and r^{-2} profile, respectively, with 215 data points. These values show reasonably good fits.

5.2 Disc mass

The SED fit shows a total dust mass of 0.03 $M_\odot$. Kemper et al. (2002) estimate a dust mass of 0.05 $M_\odot$ in the disc, from the ISO/SWS spectra. The gas mass depends on the assumed gas-to-dust ratio, but a typical ratio for circumstellar matter (100) yields 3 $M_\odot$.

We can compare this mass with that estimated from the extinction map. We use the interstellar medium (ISM) relation between the gas column density and $A_{\rm V}$

$$N(H) \approx A_{\rm V}/5.3 \times 10^{-22}\,{\rm mag\,cm^{-2}} \quad (1)$$

(Cardelli, Clayton & Mathis 1989). We assume that the region of $A_{\rm H_\alpha} > 5$ mag is the disc. We subtract the interstellar extinction

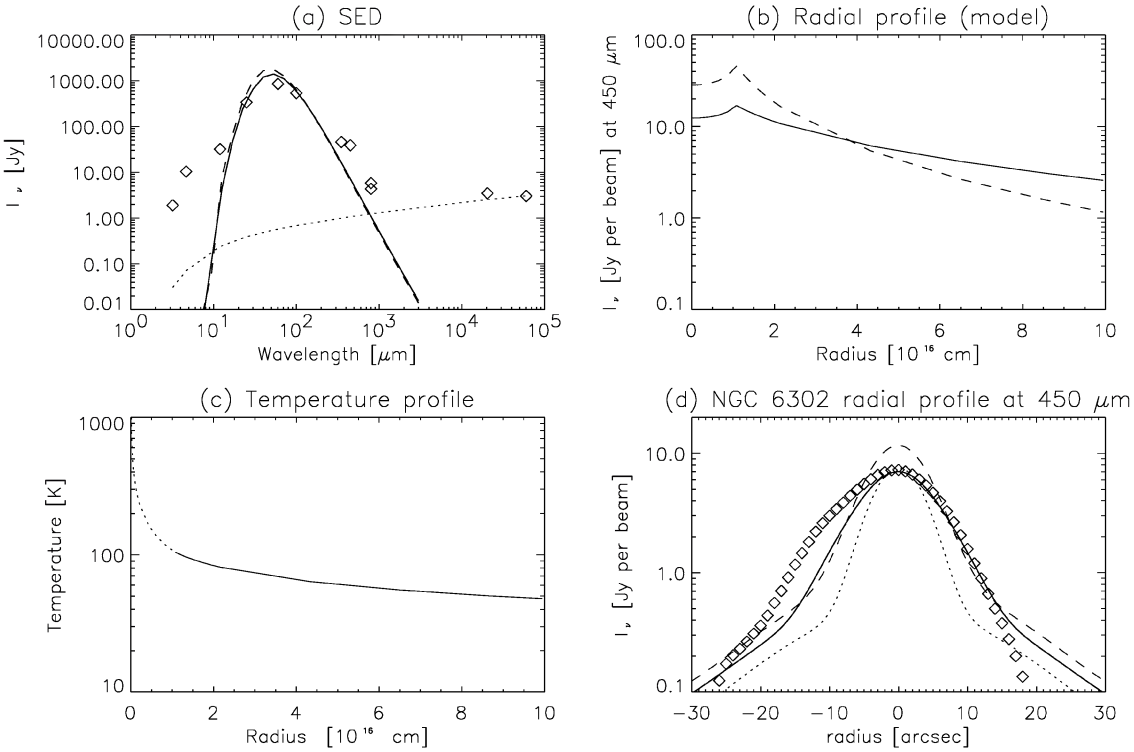

Figure 13. (a) The SED of NGC 6302 (diamonds) and model fit with two different radial profiles. The solid line is for $\rho = \rho_0\,(r/r_0)^{-1}$, and the dashed line is for $\rho = \rho_0\,(r/r_0)^{-2}$. The dotted line shows the free–free continuum. (b) Theoretical radial profiles at 450 μm. (c) Temperature profiles which do not depend on the density profile because the disc is optically thin at all wavelengths where the radiation field has significant intensity. (d) Comparison of the theoretical radial profiles for both density distributions, with the observed 450-μm profile (diamonds). The observed profile is extracted at the brightest position, in declination, equivalent Dec. The SCUBA beam profile, normalized to the observed peak flux, is plotted with a dotted line.

of $A_{\mathrm{H}_\alpha} = 0.91$ mag, and assume $A_{\mathrm{H}_\alpha} = 1.21\ A_{\mathrm{V}}$. Integrating A_{H_α} over the region of $A_{\mathrm{H}_\alpha} > 5$ mag, and doubling the result because only the foreground disc contributes to the observed extinction, we obtain a disc mass of at least 0.10 $\mathrm{M}_\odot$. The $0 < A_{\mathrm{V}} < 5$ mag region in Fig. 9 gives a mass in the lobes of 0.4 $\mathrm{M}_\odot$. In total, there is at least 0.5 $\mathrm{M}_\odot$ in the central 17.8×17.8 arcsec^2 region of NGC 6302.

The extinction mass is six times smaller than the SED mass. There are three possible reasons. First, the extinction mass may be underestimated. As discussed in Section 4.2, the extinction can be underestimated at Hα if there is ionized gas in front of thick dusty disc. Secondly, the extinction maps cannot measure the parts of the disc which extent beyond the ionized region. The 'missing mass' scales roughly proportional with size (the disc extends beyond the ionized region only in the north–south direction). The SED model gives an outer radius twice as large as the ionized shell, so that the 'extinction' mass may be underestimated by a factor of about 2. Third, the SED fitting may also have overestimated the total mass, if the far-infrared dust emissivity is much larger than assumed. (This could be the case for large, fluffy grains, but this case may also increase the required dust mass in the disc to reproduce the observed extinction.)

The mass estimated from the CO line (Huggins et al. 1996) is 0.02 $\mathrm{M}_\odot$ at the distance of 1.0 kpc, assuming the CO $J = 2$–1 line is optically thin. The large discrepancy with the CO mass is unexplained: the optical depth may be high or the CO may have frozen out on the dust grains within the dense disc. This CO mass could be considered as a lower limit. Gómez et al. (1989) estimate the molecular hydrogen mass from as ~0.1 $\mathrm{M}_\odot$, scaled to our assumed distance of 1 kpc. They find an ionized mass in the central region of $m_{\mathrm{H\,II}} = 0.02\ \mathrm{M}_\odot$. The total ionized mass is likely much higher (Pottasch & Beintema 1999) with a large amount of mass in the extended low-density wings. Our observations indicate a the disc mass of the order of 1 $\mathrm{M}_\odot$.

5.3 Disc structure

The images show evidence for complicated structures in the disc. The SED fit favours a radial density distribution of $\rho = \rho_0\,(r/r_0)^{-1}$. But in addition to the radial structure, there is also a north–south asymmetry, and indications for multiple outflow axes or warping.

Evidence for a north–south asymmetry comes from the extinction maps, where the northern region shows higher extinction. More mass may be located in this region. This is also the region where the 11.3-μm PAH feature is lacking. The cause of the asymmetry is not evident.

Evidence for multiple orientation axes is summarized in Fig. 14. The main disc is oriented north–south. The ionized region is oriented at 45 degrees to the disc (measured in the plane of the sky), as seen both in the radio map and in Brα. This arc is probably a projection of the ionized shell seen in Brα, and shows the dense gas nearest the star. The change of angle is also apparent in the lobes, which at different distances from the centre show different orientations. The outer bipolar wings are perpendicular to the dark lane (Meaburn & Walsh 1980), while the inner parts of the wings line up with the ionized region. Bipolar outflows are constrained and focussed by

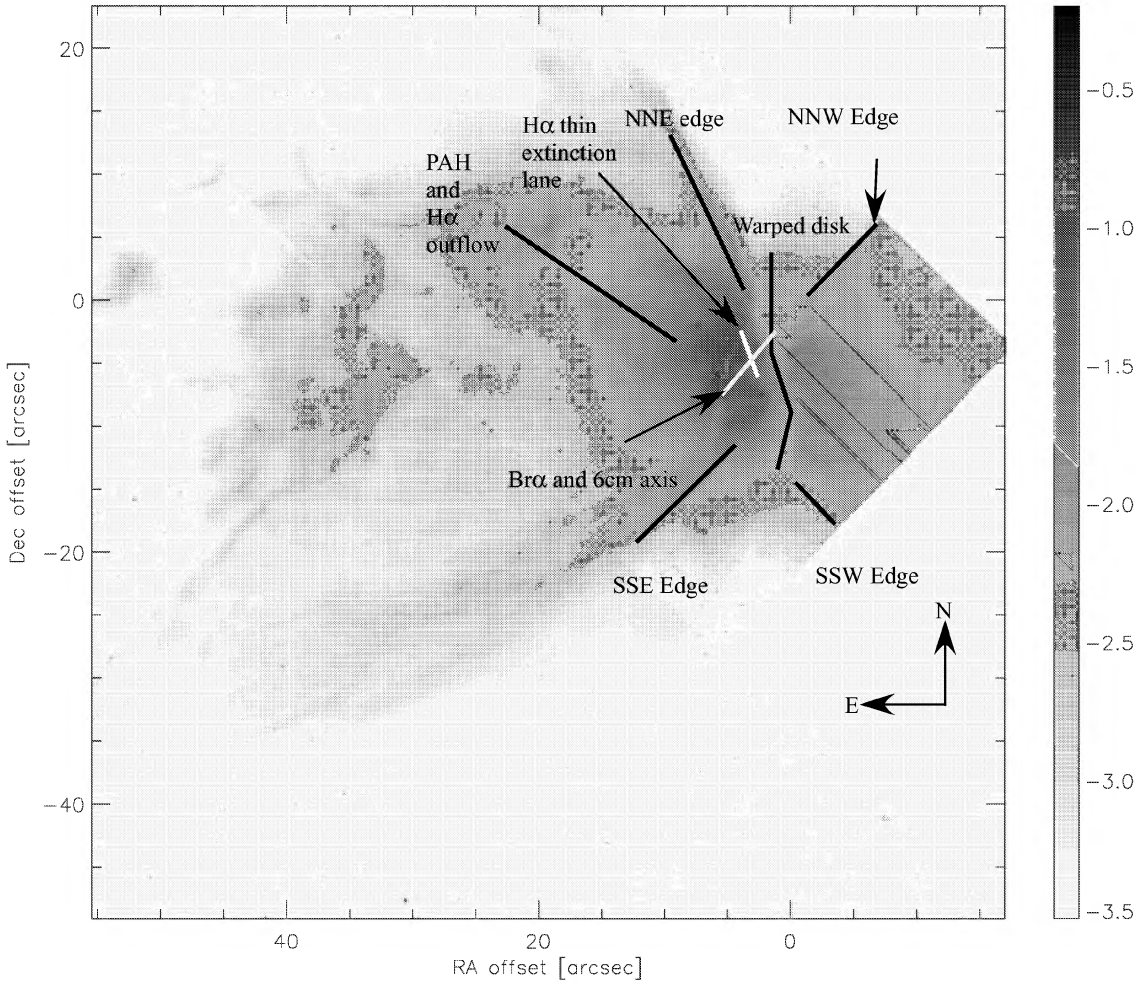

Figure 14. Warped disc and multiple axes found around the disc. The various axes of symmetry are plotted on the Hα image. The innermost, bright Hα region shows the same axis as the Brα and 6 cm continuum images, but the Hα outflow in the outer region has an axis almost perpendicular to that of the inner region. The edges of the bipolar wings are not perpendicular to the Hα outflow.

equatorial density enhancements or by discs. The varying axes at different distances can be interpreted as a significant change in angle of the constraining structure (i.e. the dark lane) with distance from the star. Processing outflows provide a possible alternative explanation, but still require a change in angle of the disc, albeit over time rather than distance. (There is, however, no evidence that the dark lane is in rotation.)

Finally, the *HST* image shows a thin lane offset from the main disc. It appears to be smaller than the main disc. This lane is oriented along the minor axis of the ionized shell.

Overall, there is strong evidence for a change in angle of the disc with distance from the centre or with time (in an expanding structure the two are closely related), which is mirrored by the outflows. The innermost dense gas, in and around the ionized shell, is rotated by 45 degrees compared to the dense gas further out. If both are part of the same structure, the implication is that the disc shows a range of angles.

Icke (2003) models the interaction of a hot stellar wind with a warped disc (Pringle 1996). The structures develop multipolar axes, and are remarkably similar to those seen in NGC 6302. At the place where the disc bends away from the plane, the stellar wind breaks though the disc in Icke's model, resulting in separate inner and outer discs, oriented at different angles. Further out, the stellar wind compresses the disc on one side: the northern arc seen in NGC 6302 can be interpreted as such a structure. Finally, the model develops a collimated flow where the fast wind breaks through the bend in the disc. The *HST* image shows faint Hα emission north–north-west (NNW) and south–south-east (SSE) (Fig. 14) of the disc, at the place where the models of Icke show this developing collimated flow. We conclude that the warped-disc model includes many of the features, such as the multiple axes, seen in the images.

5.4 Age

Discs seen around post-AGB stars, such as the Red Rectangle (HD 44179), are believed to be long-lived, surviving over $>10^4$ yrs (Waters, Trams & Waelkens 1992; Jura, Balm & Kahane 1995). Evidence for this comes from the chemistry: the discs show oxygen-rich gas while the polar outflows and the star are carbon rich. These discs date from a previous evolutionary phase, before the star became a carbon star.

The disc of NGC 6302 does not appear to be of this type. It is highly massive and is likely expanding (Payne et al. 1988), because a Keplerian disc of such mass would require a very high angular momentum. Assuming an expansion velocity of 20 km s^{-1}, the inner radius (1×10^{16} cm; Section 5.1) corresponds to an age of only 160 yr. The outer radius dates back 1600 yr. A total mass of 1 $M_\odot$ translates to a mass-loss rate over this time of $\dot{M} = 7 \times 10^{-4}\,M_\odot$ yr^{-1}. A lower expansion velocity would yield longer time-scales and lower mass-loss rates.

The highest mass-loss rates reached on the AGB over extended periods are a few times $10^{-4}\,M_\odot$ yr^{-1} (Siebenmorgen et al. 1994). The values derived for NGC 6302 are consistent with this, but we stress that neither the total mass nor the disc expansion velocity are well known. The mass derived from the SED models would yield unexpectedly high mass-loss rates, unless the time-scales are several times longer than assumed here.

The disc is stable against the fast wind from the central star, as proven by its existence. This can be understood by comparing the momenta in the disc and in the fast wind, respectively $\rho_d \Delta v_d$ and $\rho_w v_w$, where ρ_d and ρ_w are the density of the disc and outflow, and v_d and v_w are the expansion velocity of the disc and PN fast wind. v_w is taken as 1200 km s^{-1} (Meaburn & Walsh 1980) (this value requires confirmation, as discussed above). We ignore the energy loss, and assume that the collision of the PN fast wind increases the disc expansion velocity. If the density of the inner disc is $\rho_0 = 4.75 \times 10^{-18}$ g cm^{-2} [for $\rho = \rho_0\,(r/r_0)^{-1}$; Section 5.1] and $\rho_w \sim 10^4$ cm^{-3}, the increase in the expansion velocity of the disc is 2×10^{-3} km s^{-1}, which is negligible.

The lobes extend several arcmin from the star. A radius of 2.5 arcmin corresponds to a size of 2×10^{18} cm. To reach this over a time-scale of 1600 yr requires an expansion velocity of 400 km s^{-1}. The observed radial velocities range from 50 to 150 km s^{-1}. The nebula may be a few times older than assumed above.

6 AN INFRARED SOURCE NEAR THE CENTRAL STAR

The central star of NGC 6302 has not previously been detected (Pottasch & Beintema 1999) in direct images. Feibelman (2001) and Groves et al. (2002) claim scattered light of the central star in their spectra, but the star itself lies in a region of high extinction.

In the M_NB, NB_4.07, and NB_3.21 images (Fig. 2 and 3), a compact source is present near the centre of symmetry of the infrared and radio images [position (g) in Fig. 9]. It has no counterpart at Hα, suggesting high optical depth or non-ionized gas. The source is located at or near the centre of the rectangular cavity which is seen in Fig. 2 and in the radio image (Fig. 5). The compact source could therefore be located near to the central star.

The flux of the compact source, using 0.355-arcsec aperture photometry, is 10.6 ± 0.4, 11.4 ± 0.3 and 13.8 ± 0.5 in magnitudes in M_NB, NB_4.07 and NB_3.21. The ISAAC point spread function has a long tail; with such a small aperture of 1 FWHM, the photometric accuracy may not be high. We measure the aperture correction from nearby stars in the same field as NGC 6302, to remove the seeing dependence.

The source is likely to be related to the central star itself, however, the measured magnitude does not show the flux from the star solely. The stellar temperature, estimated from Zanstra temperatures or from ionization equilibrium, is in the range 1×10^5–4.3×10^5 K (Ashley & Hyland 1988). The IR photometry, for a temperature of 1.0×10^5 K gives a luminosity $L = 4.8 \times 10^4\,L_\odot$. This luminosity would be consistent with the evolutionary track for stars with initial mass of $5.0\,M_\odot$ (Vassiliadis & Wood 1993; Blöcker 1995). But if the temperature is higher, the resultant luminosity increases dramatically. The infrared fluxes also show an extremely red colour. This suggests the extinction should not be ignored, and the luminosity could be even higher. The measured flux could be affected by dust emission or free–free and bound–free emission from a stellar wind.

We obtained *L*-band spectra of NGC 6302 with ISAAC on 2004 April 30. Across the central object, we detect hydrogen recombination lines and a 3.94-μm emission line, while the other regions along the slit do not show a 3.94-μm line at all. There is a clear difference in the spectra towards the central object. This confirms the existence of the central source but does not explain the origin of the infrared excess. The 3.94-μm emission line is identified as Si IX by Beintema & Pottasch (1999), Casassus et al. (2000), although it could be the Fe II line which is of photospheric origin in O-type stars (Lenorzer et al. 2002). We therefore tentatively identify the source with emission associated with the central star, but the continuum emission is unlikely to be photospheric. A Be-type disc could be considered.

7 CONCLUSION

The optical and infrared images show the complicated structures near the core of NGC 6302. The infrared data and associated extinction maps show evidence for a central cavity which is hidden at optical wavelengths by high extinction. An ionized shell surrounds the central cavity, in which the star is located. An infrared source of unknown origin is detected at this position. The shell is ionization bounded in the N–S direction, as indicated by the PAH extent. The presence of ionized lobes extending in the east–west direction implies that the inner shell is ionization bounded in this direction, which is also suggested by the fact that the PAH extent is the same as that of the ionized gas in this direction.

NGC 6302 has internal extinction, and this has complicated structure. The dark lane shows extinction of 5–6 mag at Hα and 1–2 mag at Brα. The SED fit yields a disc dust mass of $0.03\,M_\odot$. There is some uncertainty owing to the dust emissivity and gas-to-dust ratio, but the gas-to-dust ratio for the ISM suggests $3\,M_\odot$. The extinction map gives about $0.5\,M_\odot$, assuming the relation of the extinction and hydrogen mass for the ISM, but this may be a lower limit. There could be a massive disc in NGC 6302, with mass of the order of $1\,M_\odot$. The SED fit favours a radial density distribution of $\rho \propto r^{-1}$.

The orientation of axes shows a marked change with distance from the star, with the ionized shell rotated by 45 degrees in the plane of the sky, compared to the main disc. There is a inner dark lane oriented along the approximate minor axis of the ionized shell. The change of orientation is mirrored by the outflow. Several of the structures are similar to those predicted in the warped-disc model of Icke (2003). NGC 6302 may therefore be a good test case for this model.

ACKNOWLEDGMENTS

We are grateful for the support by the ESO staff, both in preparing the observations (thanks Fernando!) and carrying out the observations. The ESO/ST-ECF Science Archive, VLA archive, ISO archive and JCMT archive were used for this research. The JCMT is operated by the Joint Astronomy Centre on behalf of the UK Particle Physics and Astronomy Research Council (PPARC), the National Research Council of Canada and the Netherlands Organization for Pure Research. We thank the referee Dr Casassus for his comments,

and showing unpublished data. Drs T. Onaka and F. Kemper stimulated discussion about dust grains. M.M. thanks Dr J.V. Buckle for rescuing her from difficulties in data reduction. This research was financially supported by a PPARC rolling grant.

REFERENCES

Adams F. C., Shu F. H., 1985, ApJ, 296, 655
Adams F. C., Shu F. H., 1986, ApJ, 308, 836
Anderson J., King I. R., 2003, PASP, 115, 113
Ashley M. C. B., Hyland A. R., 1988, ApJ, 331, 532
Balick B., 1987, AJ, 94, 671
Balick B., Frank A., 2002, ARA&A, 40, 439
Beintema D. A., Pottasch S. R., 1999, A&A, 347, 942
Blöcker T., 1995, A&A, 299, 755
Bohigas J., 1994, A&A, 288, 617
Cardelli J. A., Clayton G. C., Mathis J. S., 1989, ApJ, 345, 245
Casassus S., Roche P. F., Barlow M. J., 2000, MNRAS, 314, 657
Dudziak G., Walsh J. R., 1997, in Casertano S., Jedrzejewski R., Keyes Ch. D., Stevens M., eds, The 1997 HST Calibration Workshop with a New Generation of Instruments. Space Telescope Science Institute, p. 338
ESO Press Release, 06, 1998
Feibelman W. A., 2001, ApJ, 550, 785
Gesicki K., Zijlstra A. A., 2003, MNRAS, 338, 347
Gómez Y., Rodríguez L. F., Moran J. M., Garay G., 1989, ApJ, 345, 862
Groves B., Dopita M. A., Williams R. E., Hua C. T., 2002, PASA, 19, 425
Hoare M. G., Roche P. F., Clegg R. E. S., 1992, MNRAS, 258, 257
Hogerheijde M. R., Sandell G., 2000, ApJ, 534, 880
Holland W. S. et al., 1999, MNRAS, 303, 659
Huggins P. J., Bachiller R., Cox P., Forveille T., 1996, A&A, 315, 284
Hummer D. G., Storey P. J., 1987, MNRAS, 224, 801
Hummer D. G., Storey P. J., 1995, MNRAS, 272, 41
Icke V., 1988, A&A, 202, 177
Icke V., 2003, A&A, 405, L11
Jura M., Balm S. P., Kahane C., 1995, ApJ, 453, 721
Kastner J. H., Li J. Q., Vrtilek S. D., Gatley I., Merrill K. M., Soker N., 2002, ApJ, 581, 1225
Kemper F., Molster F. J., Jäger C., Waters L. B. F. M., 2002, A&A, 394, 679
Kwok S., 1982, ApJ, 258, 280
Kwok S., 2000, The Origin and Evolution of Planetary Nebulae. Cambridge Univ. Press, Cambridge
Lenorzer A., Vandenbussche B., Morris P., de Koter A., Geballe T. R., Waters L. B. F. M., Hony S., Kaper L., 2002, A&A, 384, 473
Lopez B., Tessier E., Cruzalebes P., Lefèvre J., Le Bertre T., 1997, A&A, 322, 868
López-Martín L., Raga A. C., Mellema G., Henney W. J., Cantó J., 2001, ApJ, 548, L288
Lord S. D., 1992, NASA Technical Memor., 103957
Mathis J. S., 1999, Allen's Astrophysical Quantities, 4th edn. Springer, Berlin
Meaburn J., Walsh J. R., 1980, MNRAS, 193, 631
Mennickent R. E., Vogt N., 1988, A&AS, 74, 497
Milne D. K., Aller L. H., 1975, A&A, 38, 183
Milne D. K., Aller L. H., 1982, A&AS, 50, 209
Molster F. J., Yamamura I., Waters L. B. F. M. et al., 1999, Nat, 401, 563
Moorwood A., Cuby J. G., Ballester P. et al., 1999, ESO Messenger, 95, 1
Nomura H., 2002, ApJ, 567, 587
Nomura H., Millar T. J., 2004, A&A, 414, 409
O'Dell C. R., Balick B., Hajian A. R., Henney W. J., Burkert A., 2002, AJ, 123, 3329
Omont A., 1986, A&A, 164, 159
Payne H. E., Phillips J. A., Terzian Y., 1988, ApJ, 326, 368
Pottasch S. R., Beintema D. A., 1999, A&A, 347, 975
Pottasch S. R., Beintema D., Dominguez-Rodriguez F. J., Schaeidt S., Valentijn E., Vandenbussche B., 1996, A&A, 315, L261
Pottasch S. R., Beintema D. A., Feibelman W. A., 2000, A&A, 363, 767
Pringle J. E., 1996, MNRAS, 281, 357
Roche P. F., Aitken D. K., 1986, MNRAS, 221, 63
Roche P. F., Lucas P. W., Hoare M. G., Aitken D. K., Smith C. H., 1996, MNRAS, 280, 924
Rodríguez L. F., Moran J. M., 1982, Nat, 299, 323
Rodríguez L. F. et al., 1985, MNRAS, 215, 353
Sahai R., Trauger J. T., 1998, AJ, 116, 1357
Sahai R., Bujarrabal V., Castro-Carrizo A., Zijlstra A. A., 2000, A&A, 360, L9
Sahai R., Morris M., Knapp G. R., Young K., Barnbaum C., 2003, Nat, 426, 261
Sellgren K., Tokunaga A. T., Nakada Y., 1990, ApJ, 349, 120
Siebenmorgen R., Zijlstra A. A., Krügel E., 1994, MNRAS, 271, 449
Tokunaga A. T., 1999, Allen's Astrophysical Quantities, 4th edn. Springer, Berlin
van der Bliek N. S., Manfroid J., Bouchet P., 1996, A&AS, 119, 547
Van Winckel H., Waelkens C., Fernie J. D., Waters L. B. F. M., 1999, A&A, 343, 202
Vassiliadis E., Wood P. R., 1994, ApJS, 92, 125
Waelkens C., Van Winckel H., Trams N. R., Waters L. B. F. M., 1992, A&A, 256, L15
Waters L. B. F. M., Trams N. R., Waelkens C., 1992, A&A, 262, L37
Woodward C. E., Pipher J. L., Shure M., Forrest W. J., Sellgren K., 1989, ApJ, 342, 860
Zijlstra A. A., 2001a, Ap&SS, 275, 79
Zijlstra A. A., Chapman J. M., te Lintel Hekkert P., Likkel L., Comeron F., Norris R.P., Molster F.J., Cohen R.J., 2001b, MNRAS, 322, 280

This paper has been typeset from a TEX/LATEX file prepared by the author.